applied sciences

MDPI

Article

Numerical Method and Analysis of 3-Dimension Thin Layer Model for Plate Dew Point Indirect Evaporative Cooler

Wenhe Zhou [1,2,*], Li Wang [1,2] and Yapeng Jiang [1,2]

[1] School of Environmental and Municipal Engineering, Lanzhou Jiaotong University, Lanzhou 730070, China
[2] Key Laboratory of Railway Vehicle Thermal Engineering of Ministry of Education, Lanzhou 730070, China
* Correspondence: zwh6888@mail.lzjtu.cn; Tel.: +86-18093118050

Abstract

By itself or combining with other cooling technologies, the dew point indirect evaporative cooler (DIEC) will be the preferred solution for cooling buildings. However, there are still some gaps in the research on DIEC performance, one of which is that 3-D (3-dimensional) models and methods are not widely used to comprehensively indicate the cooling mechanism. Most of the available numerical methods adopted 1-D or 2-D models. Existing 3-D models and methods either ignore the water film and plate or are so complicated in the grid system and numerical calculation induced by huge size differences among calculation regions that their attractions are weak. A novel simplified numerical method for DIEC performance is first suggested in this paper, and then, its validity and more efficiency than an existing 3-D numerical method are verified with the help of experimental data and numerical results. Finally, the effects of structure and operating parameters on the performance of a plate DIEC are analyzed by this present method and COMSOL Multiphysics 6.3 software, especially η/η_0 (the reinforcement factor), which was innovatively introduced. Similar results to those of existing literature were obtained, which further indicated the practicability of this simplified method. In the conditions involved in this paper, a channel length of 1.5 m, a width of 4 mm, Re_{in} (the Reynolds number at the inlet) of 1483, and a (the air ratio) of 0.33 are recommended. In the condition suggested by this paper, η/η_0 is close to 1.2. In the same conditions, this proposed method reduces the number of mesh elements by approximately 58% and the wall-clock computational time by approximately 52% under the reported workstation conditions, and its value would be more obvious for more complicated problems.

Keywords: indirect evaporative cooling; Maisotsenko-cycle; three-dimensional model; thin-layer model

Check for updates

Academic Editor:
Douglas O'Shaughnessy

Received: 6 May 2026
Revised: 16 June 2026
Accepted: 18 June 2026
Published: 23 June 2026

Copyright: © 2026 by the authors. Licensee MDPI, Basel, Switzerland. This article is an open access article distributed under the terms and conditions of the Creative Commons Attribution (CC BY) license.

1. Introduction

Air-conditioning driven by the vapor-compression refrigerator has led to a high proportion of building energy consumption among the social terminal energy consumption [1,2], which is a challenge to achieve the "dual carbon" goal. The evaporative cooler is an environmentally friendly option, especially in dry areas, because it can cool air by water evaporation without a vapor compressor and chemical refrigerant [3]. The outlet air temperature of a TIEC (traditional indirect evaporative cooler) can be close to the wet bulb temperature corresponding to its inlet air, but that of a DIEC (dew point indirect evaporative cooler) can very closely approach the dew point temperature of its inlet air, which can improve energy efficiency by 20–70% than that of TIEC [4]. Among these, DIEC

in plate structure draws more attention due to its compact structure and efficiency; however, the study on its heat and mass transfer mechanisms and performance improvement is still underway. One of the reasons is that 3-D models and methods are not widely used to indicate the heat and mass transfer mechanism of DIEC. Many available numerical studies used simplified models and methods, such as one-dimensional models and 2-D models, and the attractions of existing 3-D models and methods are weak because they either directly ignored the plate and water film, or actually included the plate and water film, which resulted in completed grid system and calculation due to significant size difference among calculation regions. And so, a simplified and effective 3-D model and method for DIEC studies is imperative.

By the tests under various inlet air conditions, Ringvilaikul and Kumar [5] found that the wet bulb efficiency and dew point efficiency of a DIEC were 92–114% and 58–84%, respectively. By comparing the operational data of the countercurrent DIEC, Bruno [6] discovered that the average wet bulb efficiency and dew point efficiency of DIEC used in civil buildings were 18% and 10% higher than those in commercial buildings. Lee and Lee [7] found that the cooling capacity of the countercurrent DIEC with fins and insertions was the highest when the working air ratio was about 0.3. Through experimental research, Duan et al. [8] found that the wet bulb efficiency and energy efficiency ratio of a countercurrent DIEC could be improved by 31% and 40% than that of TIEC, respectively, compared to those of TIEC. Duan et al. [9] also concluded that the cooling load and its electricity consumption in some regions of China could be annually reduced by 53.1% and 13–58%, respectively, by replacing the vapor compression refrigerator with DIEC.

Compared to the numerical method, the result of the experiment method is more credible, but its ability to comprehensively indicate the heat and mass transfer mechanism of DIEC is weaker. However, the existing numerical models and methods still have gaps that are not satisfactory, which can be shown by the summary provided in Table 1.

Table 1. Summary of Numerical Models and Methods for Current Regenerative Evaporative Coolers.

Authors	Model Type	Working Conditions			Methods for Water Film and Plate
		Temperature	Humidity	Velocity	
Y. Chen et al. [10]	1-D	24–40 °C	30–90% RH	0.5–5 m/s	Neglecting
A. Hasan [11]	1-D	30 °C	34% RH	/	The interface thermal resistance is assumed to be zero
M. Jradi et al. [12]	2-D	25–43 °C	40% RH	0.5–6 m/s	The plate is neglected, but the water film is included.
D. Pandelidis et al. [13]	2-D	18–45 °C	20 or 70% RH	/	Including the water film and plate
Y. Wan et al. [14]	2-D	25–45 °C	15–85% RH	0.5–3.5 m/s	Neglecting
A. Pakari et al. [15]	3-D	29.2–44.2 °C	18–57% RH	/	Including the water film and plate
Y. Liu et al. [16]	2-D	25.4–38.8 °C	15.9–34.6% RH	/	Explicitly considering
J. Lin et al. [17]	2-D	30.0–40.0 °C	10.5–12.0 g/kg	1.1–1.9 m/s	Including the water film and plate
S.S. Baakeem et al. [18]	1-D	25–45 °C	0.2–0.7 g/kg	1.4–6.4 m/s	Neglecting
G. Zhu et al. [19]	3-D	30–45 °C	6–26 g/kg	1–6 m/s	Explicitly considering

Compared to those existing simplified numerical models and methods, such as 1-D, 2-D, or 3-D, but ignoring the plate and water film, the existing 3-D models and methods, including actual plate and water film, are more credible, but their attractions are not strong due to their complicated grid system and calculation. In order to simplify the mesh system and calculation of the 3-D DIEC model under similar computational accuracy, this

article will innovatively provide a 3-D full-size numerical model and method for DIEC by simplifying the plate and water film as a surface with the same thermal resistance, but not ignoring them. By comparing the results of the existing experiment and the existing 3-D numerical methods, including the actual plate and water film, the reliability and advantages of this simplified numerical method will be identified. Finally, in order to further indicate the practicability of this simplified numerical method, a numerical analysis on the performance of a plate-type DIEC will be carried out with the help of this simplified method and COMSOL software. This paper aims to provide a convenient and efficient numerical method for DIEC research.

2. Numerical Models and Methods

2.1. DIEC

As shown in Figure 1, the plate-type DIEC mainly consists of an interval layout of dry and wet channels, metal plates, a water distribution device at the top of the wet channel, a water pump, a water tank, and air fans. Driven by the pump, the circulating water is sprayed from the water distribution device, and then the water film flows down the metal plate surface, and water droplets fill the wet channel. The primary air first flows and cools down through the dry channels to become the product air at the end of the dry channels, and then, a part of the product air leaves DIEC to cool the room environment. Another part of the product air enters the wet channels to transfer heat and mass with the water film and droplets, which is known as the secondary air or the working air. In this process, the water evaporation increases the humidity of the secondary air, cools the secondary air and the water film, and so the metal plates are also cooled. Finally, the secondary air with high humidity is discharged into the environment at the end of the wet channels. The cooling capacity caused by water evaporation is, respectively, used to cool the primary air, the secondary air, and the water film.

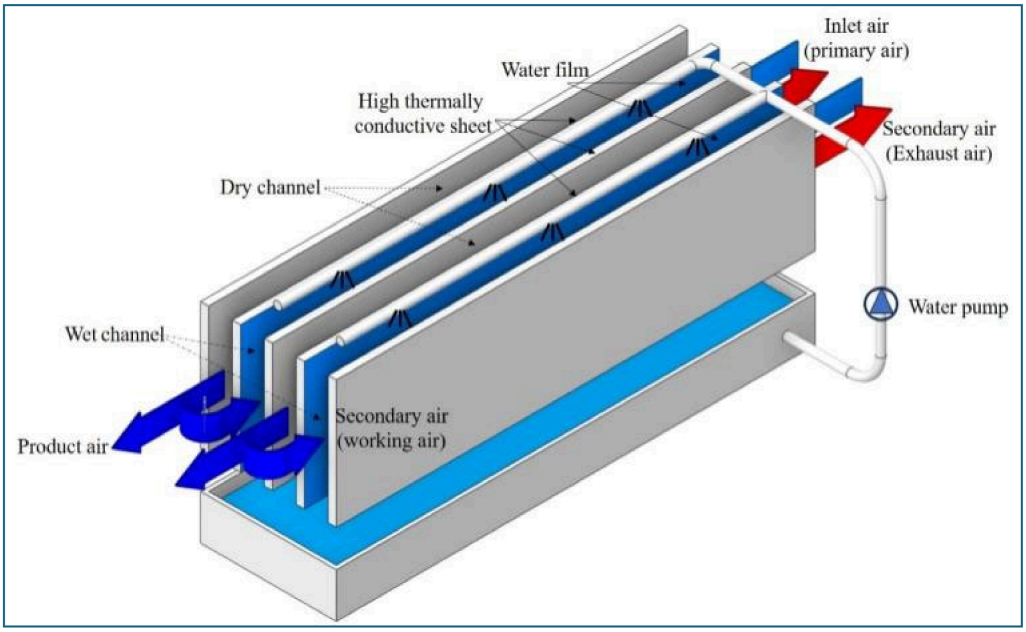


Figure 1. The plate-type DIEC.

2.2. Physical Model

Based on symmetry considerations, DIEC can be treated as a combination of heat and mass transfer units with the same function. One unit includes half a dry channel, half a wet channel, and a metal plate between them. To simplify the calculation, this paper

mainly focuses on a unit shown in Figure 2, and the overall performance of DIEC can be obtained by summing up this unit. The length of the unit model is $x = l$, the width is $y = w$, and the height is $z = h$. Based on the same plate, DIEC, B. Riangvilaikul [5] carried out an experimental study, and Guangya Zhu [19] provided a 3-D model and method including an actual plate and water film and evaluated its performance. In order to verify the validity of the simplified 3-D method provided in this paper, and to indicate its advantage over the existing 3-D method, including actual plate and water film, the same DIEC provided by B. Riangvilaikul [5] and Guangya Zhu [19] will be considered in this paper. The same structural size of one unit is shown in Table 2.

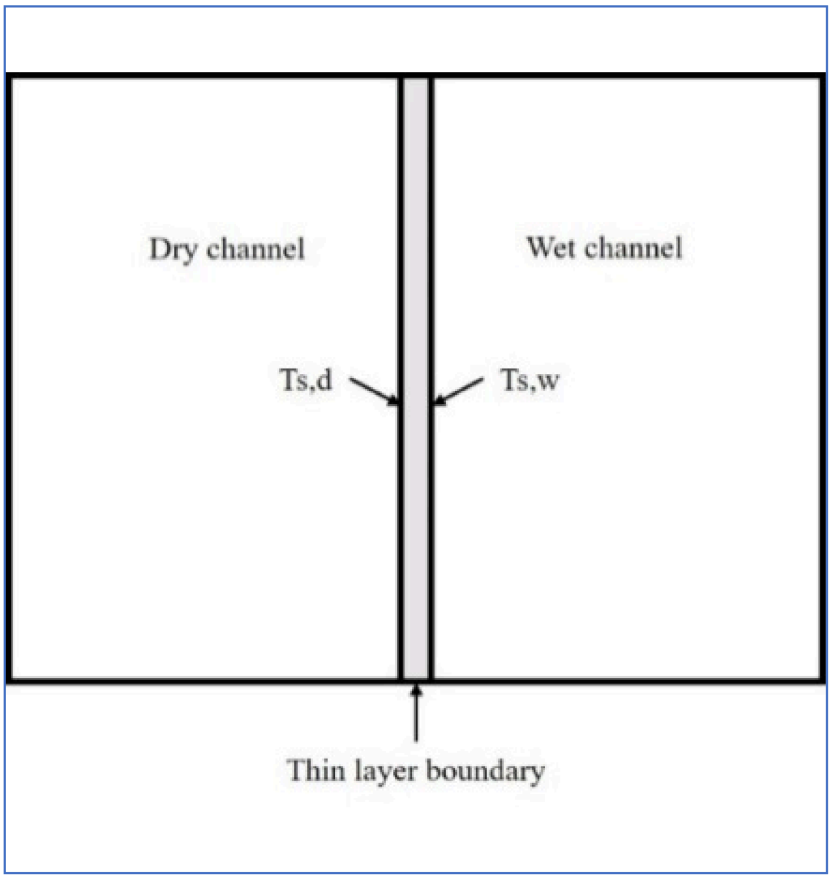


Figure 2. The heat transfer unit.

Table 2. Structural parameters of the model.

Structure	Parameters	Unit
Channel length (l)	1.2	m
Channel width (w)	5	mm
Channel height (h)	80	mm
Sheet thickness	0.5	mm
Film thickness	0.3	mm

2.3. Equations and Numerical Method

2.3.1. Thin Layer Simplification Method

In Figure 2, the plate and water film between channels are simplified as a surface with little thickness and the same thermal resistance as them. The total thermal resistance between both channels includes the thermal resistances caused from the surface convection ($h_d = h_w$, heat transfer coefficient at both surfaces is about 50 W/(m^2·K)), and the

thermal conduction of the aluminum plate (δ_a/λ_a, 0.5 mm thickness and thermal conductive of 205 W/(m·K)) and water film (δ_w/λ_w, 0.3 mm thick and thermal conductive of 0.6 W/(m·K)). And so, the plate and water film will be simplified as a surface with a total thermal resistance of 0.0405 m^2·K/W in this paper according to Equation (1). In the conditions considered in this paper, the relative error of the total thermal resistance induced by neglecting the plate and water film is less than ±3%, which would finally result in an error of calculation resulting in less than 6% when the total cooling capacity is constant.

$$R_t = \frac{1}{h_d} + \frac{\delta_a}{\lambda_a} + \frac{\delta_w}{\lambda_w} + \frac{1}{h_w} \quad (1)$$

The heat flux is one dimension along the plate and water film thickness direction, as described in Equation (2).

$$-n \cdot q = \frac{\lambda_s}{\delta_s}(T_{s,w} - T_{s,d}) \quad (2)$$

where q is the cooling capacity per unit area obtained by the product air, $\boldsymbol{n}$ is the normal direction of q, $T_{s,w}$, and $T_{s,d}$ are the wall temperatures of plate sides respectively, δ_s and λ_s are the plate and water film thickness and their thermal conductivity, respectively.

2.3.2. Numerical Methods

In this paper, COMSOL Multiphysics 6.1 software is used. The numerical calculation process is illustrated in Figure 3. In order to simplify the numerical study of the unit model coupled with heat and mass transfer, the following assumptions are predefined.

(1) In the conditions considered in this paper, the air is considered as a weakly compressible fluid, which means that the air density and specific heat depend on the air temperature and humidity, shown as Equations (3) and (4) in the ranges of 25–45 °C and 6.9–26.4 g/kg humidity involved in this paper. This can avoid the relative error of the calculation results of about 2.5% if the average air density is used.

$$\rho = \frac{101,325(1+d)}{287T(1+0.6226d)} \quad (3)$$

$$c_p = 1.005 + 1.86d \quad (4)$$

(2) The airflow in the channels is laminar due to the small air velocity and Reynolds number.

(3) Considering the outer surface area of DIEC is much smaller than its heat transfer area, and its shell is well insulated by a 50 mm thickness of foam plate (thermal conductivity is about 0.036 W/(m·K)), the exchange of heat and mass between DIEC and the surrounding environment is neglected in this paper, which could induce an error of less than 1%.

(4) DIEC works under steady-state conditions, including the water film thickness and the surface temperature. Although the water film thickness along the wet wall is not constant, the result of the error induced by the assumption of the thin film thickness is less than 1%, because the ratio of the water film resistance to the total thermal resistance is less than ±3%, and the error resulting from the dry area on the wet surface is about 10% [19]. Because the heat transfer capacity depends only on the temperature difference between channels, the total thermal resistance, and the heat transfer area, the assumption of a continuous and uniform water film is acceptable in the parameter range involved in this paper.

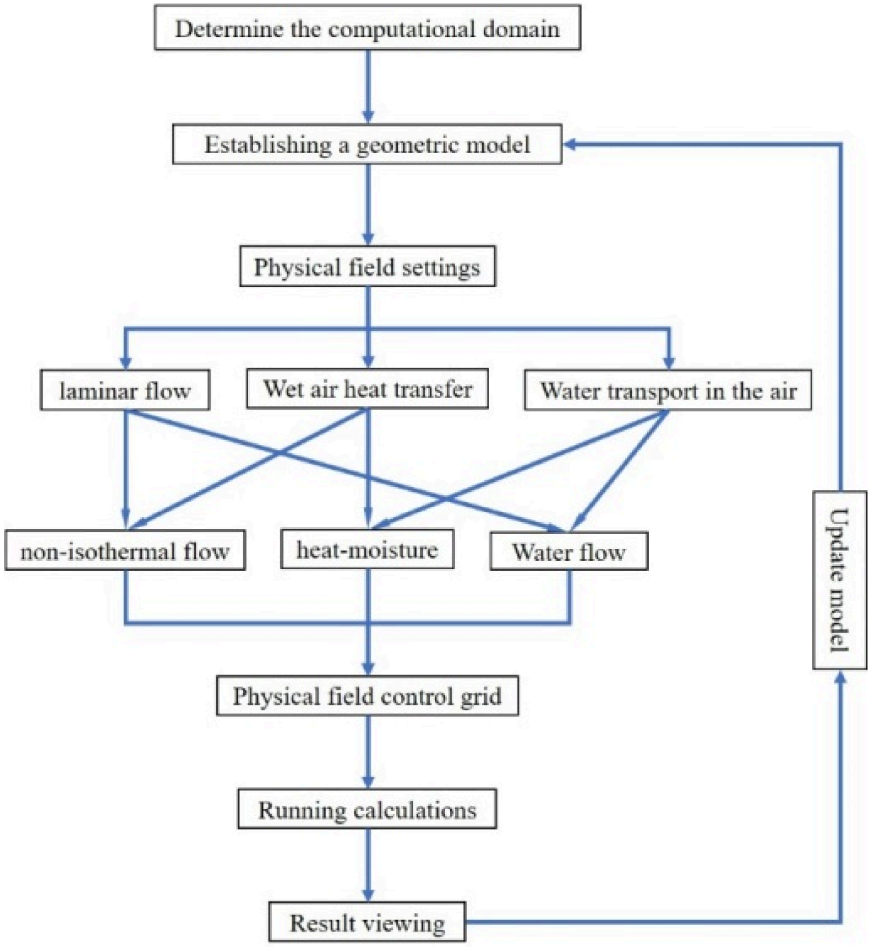


Figure 3. 3-D numerical simulation flowchart.

2.3.3. Numerical Equations

The numerical calculation is based on the Ringvilaikul and Kumar model [4] and the following control Equations (5)–(8), which are the continuity equation for airflow, the momentum equation, the Energy conservation equation, and the water diffusion equation, respectively.

$$\frac{\partial \rho}{\partial t} + \nabla \cdot (\rho \mathbf{U}) = 0 \tag{5}$$

$$\rho \frac{\partial \mathbf{U}}{\partial t} + \rho \mathbf{u} \cdot \nabla \mathbf{U} = -\nabla p + \nabla \cdot \tau + \mathbf{F} \tag{6}$$

$$\rho C_p \left(\frac{\partial T}{\partial t} + \mathrm{u} \cdot \nabla T \right) + \nabla \mathrm{q} = 0 \tag{7}$$

$$M_v \frac{\partial C_v}{\partial t} + M_v u \cdot \nabla C_v + \nabla (-M_v D \nabla C_v) = 0 \tag{8}$$

The saturation concentration of water vapor in the air is defined by Equation (11) based on the assumption of an ideal gas, where T is the water film temperature, and $P_{sat \cdot T}$ is defined as Equation (12).

$$\tau = \mu \left(\nabla \mathbf{u} + (\nabla \mathbf{u})^T \right) - \frac{2}{3} \mu (\nabla \cdot \mathrm{u}) \mathbf{I} \tag{9}$$

$$C_v = \varphi_w C_{v \cdot sat} \tag{10}$$

$$C_{v\cdot sat} = \frac{P_{sat\cdot T}}{RT} \tag{11}$$

$$P_{sat\cdot T} = 610.7 \times 10^{7.5\frac{T-273.15}{T-35.85}} \tag{12}$$

2.3.4. Evaluation Indicators

In this paper, DIEC performance is evaluated by the dew point efficiency η_{dp} defined by Equation (13), and the cooling capacity per unit area q defined by Equation (14). In addition, the reinforcement factor η/η_0 defined in Equation (15) is used to comprehensively assess if it is a cost-effective measure by considering additional resistance introduced in the enhancement process, of which the subscript 0 refers to the referenced DIEC provided by Y. L. He [20] and N. R. Rosaguti [21]. The resistance factor f and the heat transfer factor j are defined by Formulas (16) and (17), respectively. The power exponent 1/3 is considered here because the fan power consumption is proportional to 1/3 of the resistance loss. When η/η_0 is larger than 1, the overall performance of the improved DIEC is better than that of the referenced one, and so, the improved measure is effective.

$$\eta_{dp} = \frac{T_{dc,in} - T_{dc,out}}{T_{dc,in} - T_{dp}} \tag{13}$$

$$q = \left[c_p \dot{m}(1-a)(T_{dc,in} - T_{dc,out})\right]/A \tag{14}$$

$$\frac{\eta}{\eta_0} = \frac{j/j_0}{(f/f_0)^{1/3}} \tag{15}$$

$$f = \frac{2d_e \Delta P}{L \cdot \rho_d u_{in}^2} \tag{16}$$

$$j = \frac{Nu}{Re \cdot Pr^{1/3}} \tag{17}$$

$$\Delta P = f \cdot \frac{l}{d}\frac{1}{2}\rho_d u_{in}^2 \tag{18}$$

$$Nu = \frac{h_a d_e}{\lambda} \tag{19}$$

$$Pr = \frac{C_p \mu}{\lambda} \tag{20}$$

2.3.5. Boundary Conditions

The dry channel inlet and the wet channel outlet are defined as the unit inlet and outlet, respectively. The outlet of the dry channel is defined as an open boundary with a normal stress of zero. The plate and water film are simplified as a thin layer with little thickness. The water film surface is defined as a wet surface. The boundary conditions are detailed in Table 3.

Table 3. Boundary Condition Setting Table.

Boundary Name	Set Region	Specific Settings
Primary air inlet	$x = 0, 0 \le y \le w/2, 0 \le z \le h$	$T = T_{in}, u = u_{in}, \varphi_w = \varphi_{in}$
Primary air outlet	$x = l, 0 \le y \le w/2, 0 \le z \le h$	$p_e = 0$
Secondary air outlet	$x = 0, w/2 \le y \le w, 0 \le z \le h$	$u = u_{in}(1-a)$
Symmetric boundary	$0 \le x \le l, y = 0, y = w, 0 \le z \le h$	$-\boldsymbol{n}\cdot\boldsymbol{q} = 0$
Dry channel, thin-walled	$0 \le x \le l, y = w/2, 0 \le z \le h$	$-n\cdot q = \frac{\lambda_s}{\delta_s}(T_{s,w} - T_{s,d})$
Wet channel wet surface	$0 \le x \le l, y = w/2, 0 \le z \le h$	$c_{sat} = (P_{sat}(T_f))/RT, g_v = M_v K(C_{sat} - C_v)$

2.4. Regional Discretization and Assessment of Grid Independence

In this paper, the finite element method and a structured grid system with hexahedral elements are used to discretize the physical model. The result is shown in Figure 4. The grid elements along the channel length (x-direction), the channel width (y-direction), and height (z-direction) are uniformly distributed with a size ratio of 5. The grid elements at the places with large parameter gradients are additionally refined with a size ratio of 2 to capture velocity and temperature gradients, such as the nearby plate, water film, and the wet channel inlet. A sensitivity analysis of the near-wall grid indicated that further refinement alters the local wall mass flux by less than 2%, and the maximum y+ remains below 0.5, confirming the proper resolution of the boundary layers.

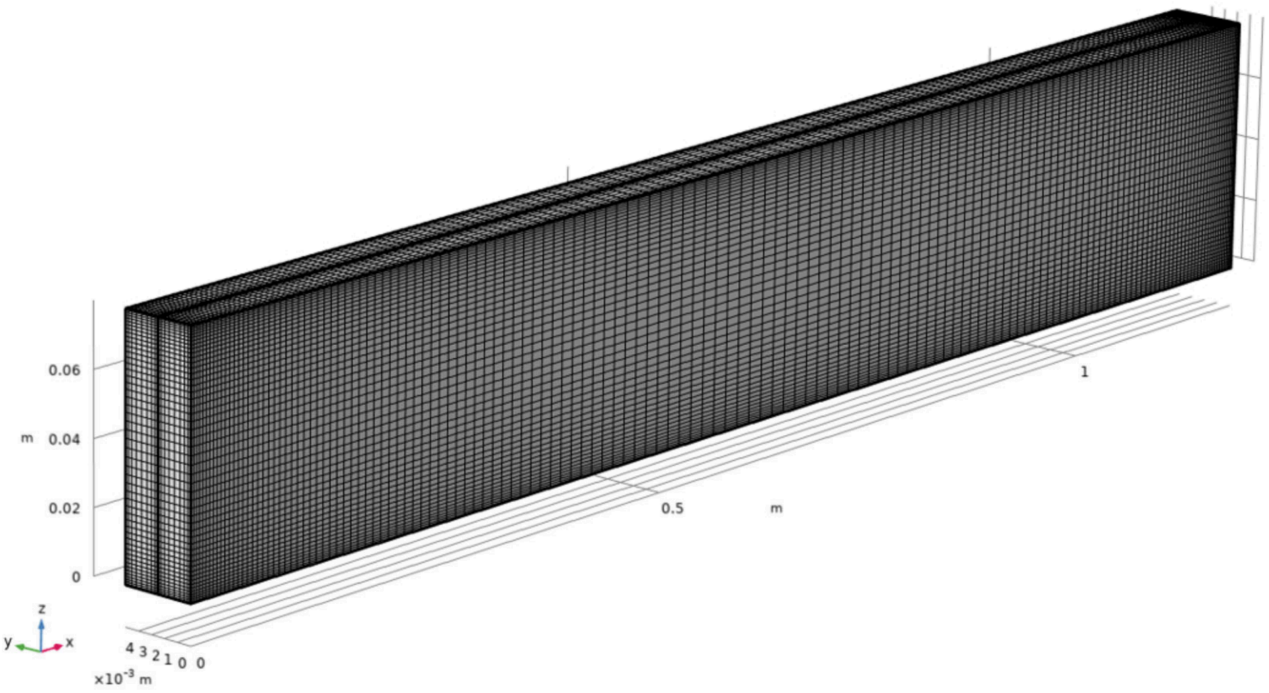


Figure 4. Grid division of the computational domain.

To look for the balance point between the calculation accuracy and the grid number, the grid systems with 50,000, 100,000, 150,000, 200,000, 250,000, and 300,000 units are used to calculate the outlet temperature of the product air respectively at the conditions of an inlet air temperature of 45 °C and absolute humidity of 6.9 g/kg, 11.2 g/kg, 20.0 g/kg, and 26.4 g/kg. The results are presented in Figure 5. It's clear that the humidity effect of the air at the inlet on the product air temperature is very obvious. Because the good cooling effect mainly depends on the low air humidity, the higher the inlet air humidity, the higher the outlet air temperature is. The numerical results are not sensitive to the grid number. Considering the accuracy of the calculation results and the conservation of computer resources, this paper finally selects the 150,000-grid system for subsequent numerical calculations, because the maximum difference between the results based on the grid system with 150,000 units and that of the grid system with 300,000 units is only 0.9%.

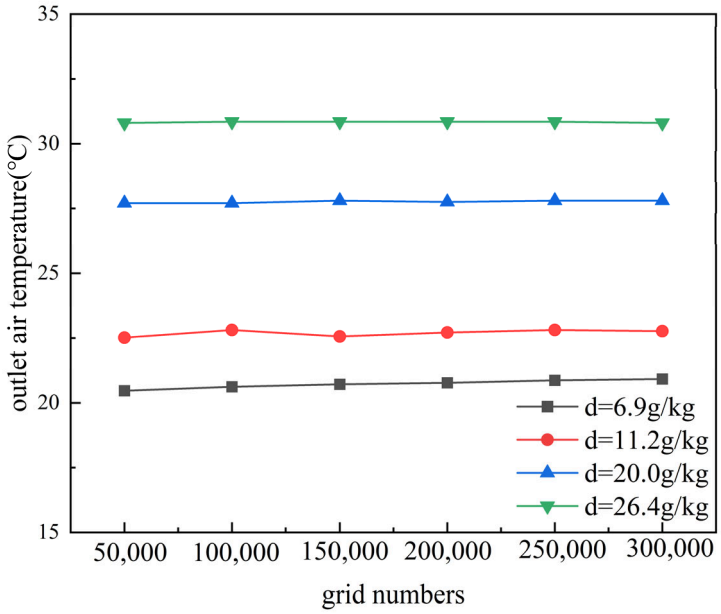


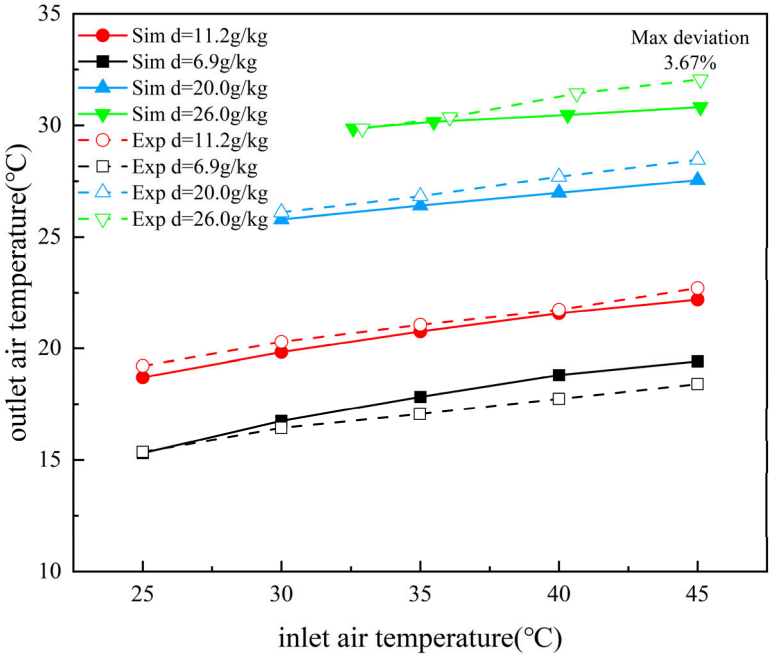
Figure 5. Independence assessment of the grid system.

2.5. Model and Method Validation

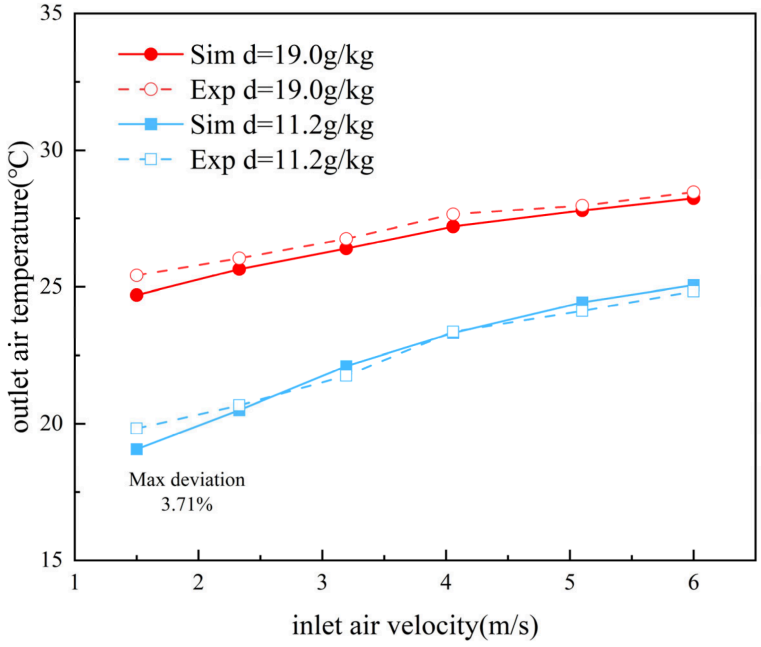
To validate the numerical model and method presented in this paper, the product air temperatures at the dry channel outlet are calculated by the numerical method provided in this paper at the conditions shown in Table 4, which is the same as that of B. Riangvilaikul [5] and Guangya Zhu [19]. The results calculated by this paper and the experimental data provided by B. Riangvilaikul [5] are presented in Figure 6. When the air humidity, temperature, and flow rate at the inlet increase, both results at the dry channel outlet show similar increasing trends, especially in the low humidity range. Under the same inlet temperature and humidity conditions, the maximum deviation of both product air temperatures at the dry channel outlet shown in Figure 6a is 3.67%, and the average value is 0.33%. Similarly, under the same intake speed conditions, Figure 6b shows that the maximum deviation between the calculated one and the experimental data in B. Riangvilaikul [5] is 3.71%, and the average value is 0.6%. The deviation reason may be caused by the water film thickness. In the low air humidity conditions, the larger evaporation in the actual process of B. Riangvilaikul [5] results in a thinner water film than that of 0.3 mm, which is assumed constant in this paper, and so, a larger thermal resistance results in a smaller heat obtained by the primary air in B. Riangvilaikul [5] than that calculated by this paper. Moreover, in high-humidity conditions, the situation is contrary. The actual thickness and the thermal resistance of the water film in B. Riangvilaikul [5] are larger than that of the 0.3 mm constant assumed by this paper, especially in the low air velocity conditions, because the evaporation is smaller.

Table 4. Operating conditions.

Parameters	Value	Unit
Inlet air temperature	25~45	°C
Inlet air humidity	6.9~26.4	g/kg
Inlet air velocity	1.5~6	m/s
Working air-to-intake air ratio	0.33	kg/kg



(**a**) based on the inlet air temperature.



(**b**) based on the inlet air velocity.

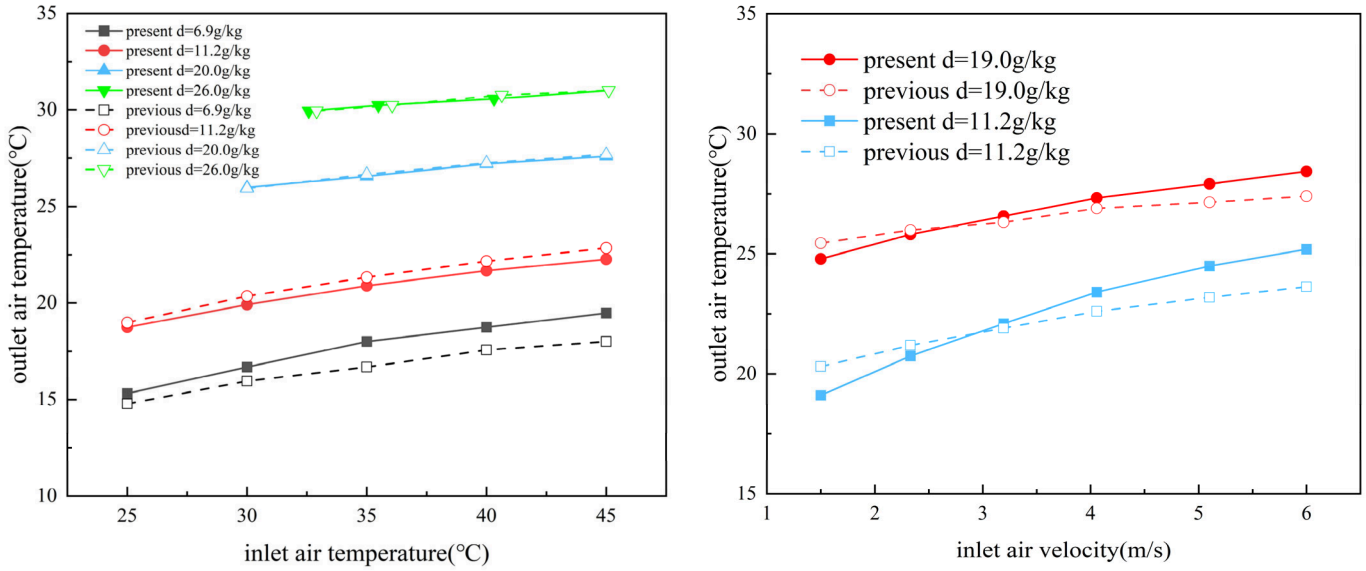
Figure 6. The verification of the model and method.

3. Results and Discussion

3.1. Evaluation of the Thin-Layer Numerical Method

In order to show the efficiency and accuracy of the present method provided by this paper in terms of computer resource conservation, the product air temperature is calculated by the present method and compared with that of the previous method provided by Guangya Zhu [19], which considered the wet wall with 10% dry area. Figure 7a shows that the product air temperatures of both methods are in agreement with each other and increase with the inlet air temperature and humidity. Compared to that in the present model, the total thermal resistance in the previous model is smaller. When the inlet air humidity is low, the evaporation in both models is large, and the effect of the thermal resistance on the

product air temperature is dominant at this time. The product air temperature in Guangya Zhu [19] is lower 8.54% than that in the present model at the inlet humidity of 6.9 g/kg and the temperature of 45 °C. Compared to the present model, the evaporation in the previous model [19] is smaller due to a 10% dry area. With the inlet air humidity increasing and the evaporation decreasing, the thermal resistance effect on the product air temperature is gradually weakened. And so, the calculation consistency of the present model with that of the previous model [19] is better and better. Figure 7b shows that the product air temperatures in both models are nearly identical as the inlet air velocity and humidity increase, and the maximum deviation is 6.89% at the inlet air humidity of 11.2 g/kg and the air velocity of 6 m/s. The thermal resistance effect on the product air temperature is obvious when the inlet air velocity and resulting evaporation are large. The product air temperature in the previous model [19] is lower than that in the present model because the primary air in the previous model [19] could obtain more cooling capacity. The results in the low-velocity range are contrary.



(**a**) based on the inlet air temperature (**b**) based on the inlet air velocity

Figure 7. Calculation result comparison between the two models.

The plate and water film is considered by Guangya Zhu [19] based on actual conditions and 10% dry area on the wet surface, and that is considered by this paper based on the simplified assumption of a surface with the same thermal resistance. For the same DEIC, both papers used the same model and software, but different methods on the plate and water film. The grid system of 357,000 is adopted by Guangya Zhu [19], while this paper adopted the grid system of 150,000 to obtain similar results, which reduces the number of mesh elements by approximately 58% and the wall-clock computational time by approximately 52% under the reported workstation conditions. For more complex evaporative coolers and similar heat and mass transfer problems, it can be anticipated that this method will present a more significant advantage in reducing computer resources, and so, facilitate the numerical calculation for similar 3-D models.

3.2. Impact of Structural Parameters

To further show the practicability of the numerical method provided in this paper, the effects of the channel length and width of DIEC on its performance are numerically calculated by changing channel width from 2 mm to 6 mm, and length from 0.5 m to 3 m,

respectively. In the calculation process, the inlet air velocity is 2.4 m/s, and a (the ratio of the secondary air to the primary air) is 0.33. The inlet parameters of DIEC referenced the meteorological parameters of summer in Lanzhou city. The dry bulb temperature presented in the design code is 31.2 °C, and the relative humidity is 38.39%RH.

Figure 8 shows the structure effects on η_{dp} (the dew point efficiency) and q (the cooling capacity per unit area). When the channel width increases at a constant length, the product air temperature at the dry channel outlet increases, and η_{dp} gradually decreases. This is because the cooling effect on the primary air decreases when the air volume increases under similar cooling capacity conditions. At short channel conditions, the η_{dp} slope is steeper as the channel width increases due to insufficient heat and mass transfer. At the same channel width conditions, η_{dp} increases when the channel length increases, but the growth trend slows down, which indicates that too long a channel is also uneconomic. In this paper, the minimum value of η_{dp} is 43.8% at the channel length of 0.5 m, and the channel width of 6 mm, and the maximum value of η_{dp} is 97.8% when the channel width and length are 2 mm and 3 m, respectively.

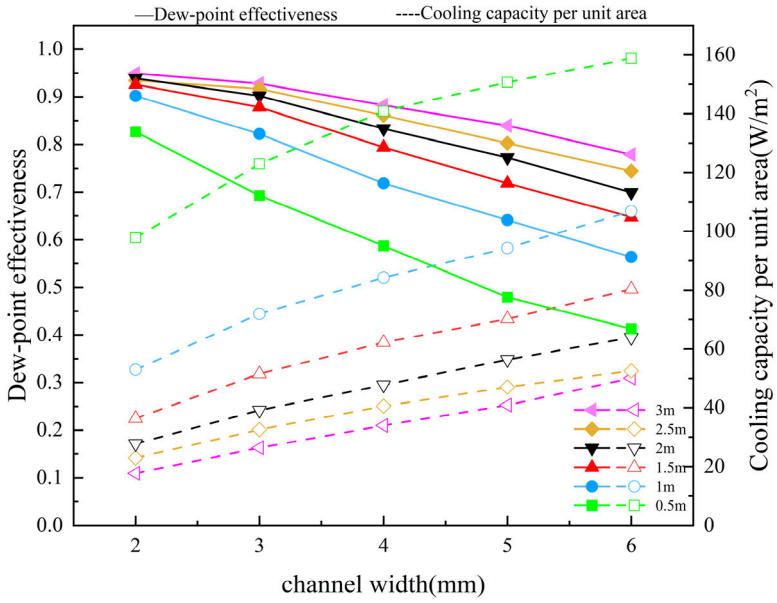


Figure 8. Structure Effects on η_{dp} and q.

When the air volume increases with the channel width, the total cooling capacity increases a little in the same plate area, and so, q increases, but when the channel width is beyond 4 mm, its impact on q gradually weakens. In the shorter channel conditions, because the average humidity difference along the wet channel between the working air and the water film is larger, and the average temperature difference between the primary air and the water film is also larger, q of the shorter channel is larger. In this paper, the maximum of q is 158.6 W/m^2 when the channel width is 6 mm, and the channel length is 0.5 m. When the channel length increases, because the total cooling capacity and its share obtained by the primary air all increase but disproportionately to the increasing area, q decreases. In this paper, the minimum value of q is 20.1 W/m^2 when the channel thickness is 2 mm, and the channel length is 3 m.

Figure 9 shows the structure effects on η/η_0 (the reinforcement factor) and ΔP (the unit resistance). At the same channel length, the resistance loss decreases when the channel equivalent diameter increases, induced by the channel width increasing, especially for those long channels less than 3 mm wide. This trend slows down when the channel width further increases beyond 4 mm, and the width effect on resistance loss is no longer significant,

especially for short channels. At the same channel width condition, the resistance loss proportionately increases with the channel length. However, when the channel width exceeds 5 mm, the length's influence on the resistance loss is no longer significant. In this paper, the minimum ΔP is 14.8 Pa at the channel width of 6 mm, and the channel length of 0.5 m, and the maximum ΔP is 488.4 Pa when the channel thickness is 2 mm, and the channel length is 3 m.

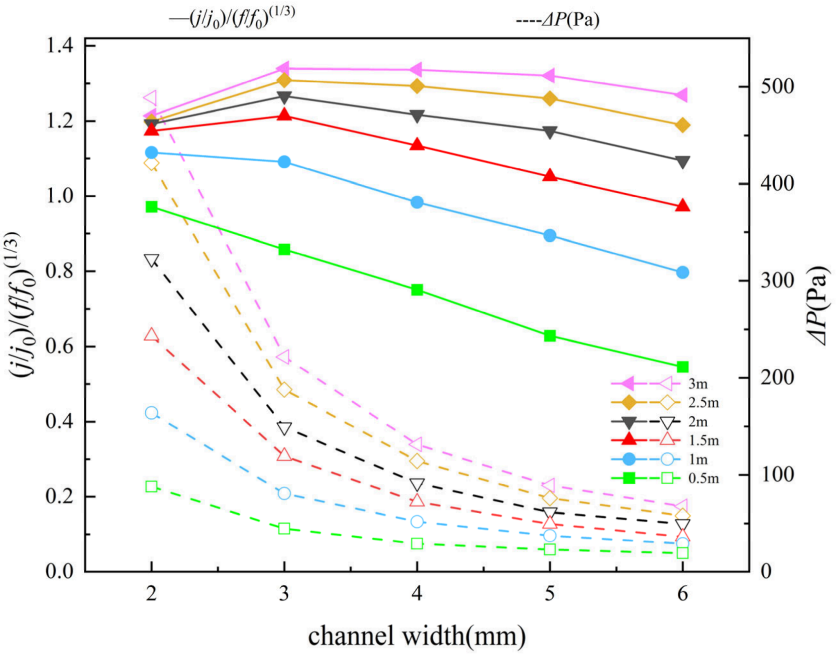


Figure 9. Structure effects on η/η_0 and ΔP.

In the conditions considered in this paper, except for the channel length of 0.5 m, η/η_0 values are all larger than 1.0, which means that the improvements in channel structure referenced in B. Riangvilaikul [5] and Guangya Zhu [19] are positive to DIEC performance. When the channel length is larger than 1.5 m, η/η_0 firstly increases with the channel width and then decreases. The maximum η/η_0 of a 4 m long channel happens at the channel width of 4 mm, and that of the other channels is at 3 mm. For the 0.5 m and 1 m long channels, η/η_0 decreases as the channel width increases. At the same channel width, the longer the channel, the better η/η_0 is. The length effect on η/η_0 is more and more significant as the channel width increases.

3.3. Effects of Air Velocity

Based on the above results, the velocity effects of the primary air and the working air on η_{dp}, q, ΔP, and η/η_0 will be indicated in this section. To do this, Re_{in} (Reynolds number of the primary air at inlet) ranges from 371 to 2224, which corresponds to air velocity of 1 m/s to 6 m/s, and a (the ratio range of the working air to the primary air) is from 0.1 to 0.6.

Figure 10 illustrates the velocity effect on η_{dp}. When more product air flows into the wet channel as a increasing at the same Re_{in}, the heat and mass transfer in the wet channel is significantly enhanced, and η_{dp} increases. However, when a increases beyond a certain value, its effect is not significant, and η_{dp} becomes flat. This is because the increase in the evaporation rate is not proportional to the increase in working airflow under the same area condition. In this paper, the maximum value of η_{dp} is 98.1% under the conditions of a of 0.6 and Re_{in} of 373. When Re_{in} increases at the same a, velocities and flows of the primary air, and the working air all increase. Although the heat exchange between the primary air

and the secondary air is improved a little, η_{dp} decreases because the same cooling capacity is allocated to more primary air. In this paper, when a is 0.1 and Re_{in} is 2224, the minimum value of η_{dp} is 32.9%.

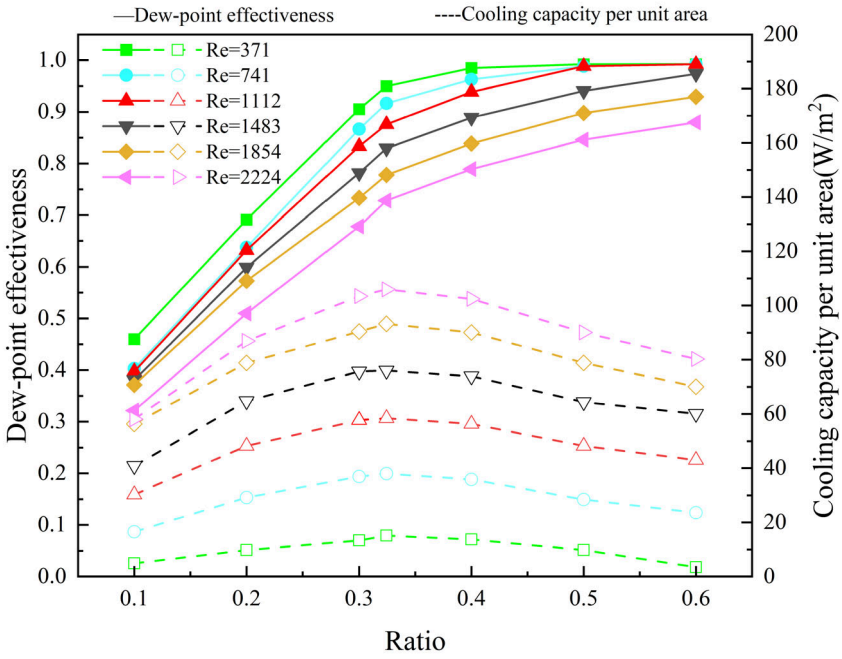


Figure 10. Operation condition effects on η_{dp} and q.

q depends on the total evaporation in the wet channel, the temperature difference, and the thermal resistance between both channels. Figure 10 also indicates the velocity effects on q. When Re_{in} and air velocity increase at the same a, q increases, but the trend gradually flattens because the total evaporation increases but not in proportion, and the thermal resistance decreases. When a increases at the same Re_{in}, total evaporation increases, and the cooling capacity obtained by the primary air increases until a = 0.33. In this paper, q reaches its maximum value of 111.37 W/m^2 at 0.33 of a and 2224 of Re_{in}. Because the total evaporation does not increase in proportion to the working air volume, when a is larger than 0.33, the working air can obtain more cooling capacity, and the cooling capacity obtained by the primary air begins to decrease. The minimum q of 14.03 W/m^2 is at 0.6 of a and 371 of Re_{in}.

ΔP includes the resistance of the dry channel and that of the wet channel. Figure 11 shows the velocity effect on ΔP. It is evident that the increase in Re results in a larger resistance. Compared to the large inlet velocity, a effects on the air resistance are not obvious when the air velocity is small. But in the larger Re_{in} conditions, ΔP significantly increases when a increases, because the resistance increase in the wet channel is obvious. In the scope of this paper, the maximum value of ΔP is 37,607 Pa when a is 0.6, and Re_{in} is 2224, and the minimum value is 39.49 Pa at 0.1 of a and 371 of Re_{in}.

Figure 11 also shows the velocity effects on η/η_0. When a is increased from 0.1 to 0.33, an obvious increase in η/η_0 is observed. That η/η_0 is larger than 1.0 indicates that the velocity increase is beneficial at an a value *of* 0.33. And if a is continually increased from 0.33 to 0.6, the obvious decrease in η/η_0 is observed. This is because the improvement in q is no longer obvious, but the increase in ΔP is positive. In this paper, the maximum value of η/η_0 is 1.14 when a is 0.33, and Re_{in} is 1483.

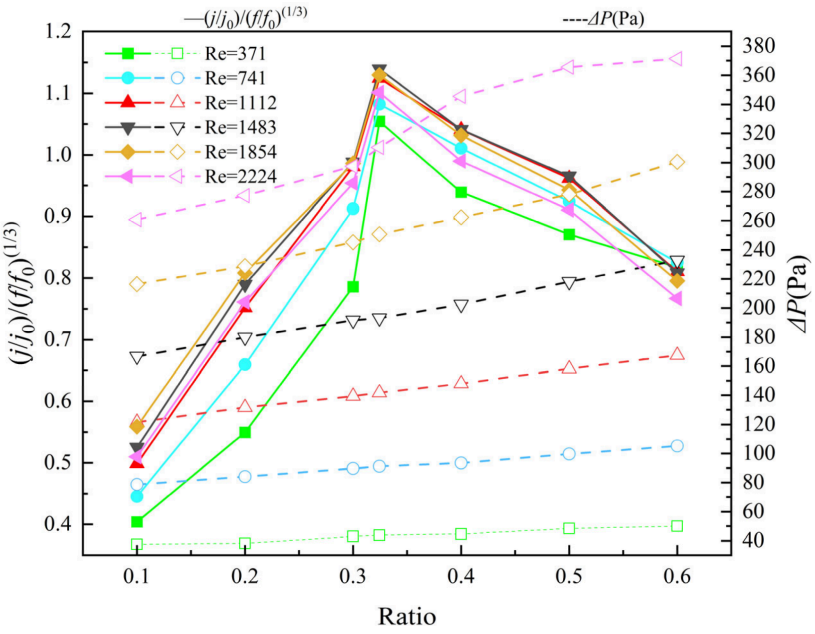


Figure 11. Operation condition effects on η/η_0 and ΔP.

3.4. Effects of Air Humidity and Temperature at the Inlet

The total cooling capacity of DIEC induced by the latent heat of water evaporation in the wet channel is used to cool the primary air, the water film, and the working air, respectively. The evaporation is driven by the vapor pressure difference between that of the water film surface (nearly 100%) and that of the working air away from the film, and so, the air relative humidity has a key effect on DIEC performance. The corresponding cloud map of temperature in the dry channel is shown in Figure 12, which vividly shows the effect of inlet air temperature. The impact of air temperature and humidity at the inlet on η_{dp} and q is indicated as shown in Figure 13, in which the inlet air temperature is between 25 °C and 45 °C and the inlet air humidity is between 10%RH and 60%RH.

When the air humidity at the inlet increases under the same conditions, q decreases because of the vapor pressure difference, and the evaporation in the wet channel decreases. Compared to the air with lower temperature, q in the condition of the higher air temperature is larger because the temperature difference is larger between the two channels. But this temperature advantage on q will not become obvious when the inlet air humidity continuously increases, and the evaporation in the wet channel decreases. In this paper, the minimum of q is 28.77 W/m^2 at inlet conditions of 25 °C and 60%RH.

There is a positive correlation between the relative humidity and the dew point temperature of air, and there is a negative correlation between the temperature and the relative humidity of air under the same conditions. Although q decreases when the relative humidity of the inlet air increases, η_{dp} increases due to the increase in the corresponding dew point temperature. When the inlet air temperature is higher, η_{dp} is larger, and its change is obvious in the low humidity range. This is because its dew point temperature is high and can be quickly approached due to a larger temperature difference. The increase of η_{dp} quickly slows down as the humidity increases at the inlet, especially in the high-temperature range. The minimum of η_{dp} is 52.3% at the condition of 10%RH/25 °C, and the maximum of η_{dp} is 98.7% at 60%RH/45 °C in this paper.

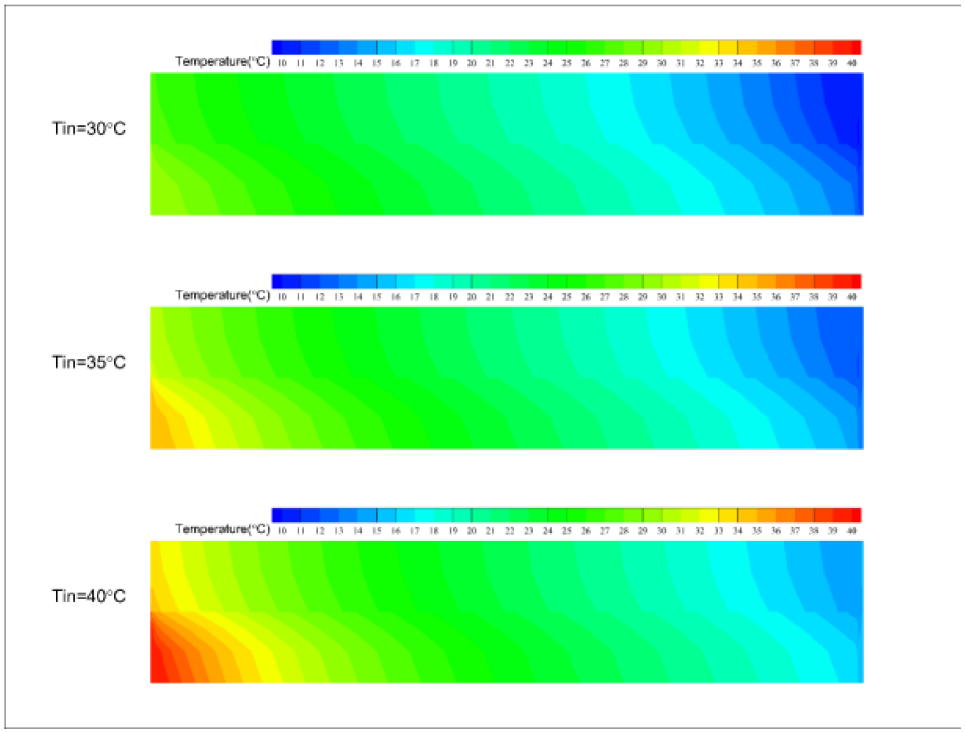


Figure 12. Cloud map of temperature in the dry channel.

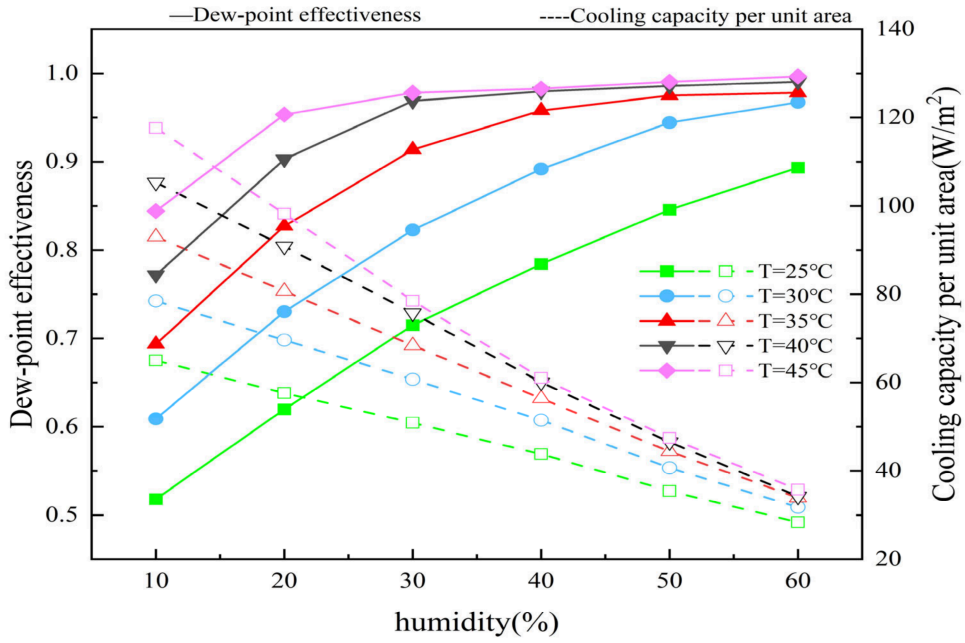


Figure 13. Air temperature and humidity effects on η_{dp} and q.

Based on symmetry considerations, DIEC can be treated as a combination of heat and mass transfer units with the same function. Although the performance of one unit is focused on in this paper, the dew point efficiency and the resistance loss of DIEC are the same, the airflow handled by DIEC is the unit airflow summation, and the cooling capacity of DIEC is the product of q and total area. In the conditions involved in this paper and Lanzhou city (the dry bulb temperature is 31.3 °C and the wet bulb temperature is 20.1 °C), the circulating water volume is usually 4–6 times the evaporation, the dew point efficiency of DIEC is about 90%, the resistance loss is about 200 Pa, the unit airflow handled is about 0.0128 m^3/s and q is about 80 W/m^2, respectively.

4. Conclusions

By simplifying the plate and water film of DIEC as a surface with the same thermal resistance but not ignoring it, this paper suggested a novel numerical method to avoid the adverse impact of huge size differences among regions on the grid system of the 3-D DIEC model. And then, with the help of the experimental data in B. Riangvilaikul [5] and the numerical results in Guangya Zhu [19], the validation and efficiency of the present method in this paper were verified. Finally, the performances of the same DIEC model as that of B. Riangvilaikul [5] and Guangya Zhu [19] were evaluated and analyzed, in which the reinforcement factor η/η_0 was innovatively introduced. The main conclusions are summarized as follows.

(1) The simplified method suggested by this paper is valid and effective in the 3-D numerical calculation of DIEC, which reduces the number of mesh elements by approximately 58% and the wall-clock computational time by approximately 52% under the reported workstation conditions. This advantage will be more obvious in solving more complex, similar problems.
(2) The similar results obtained further verified the present method in this paper. In the conditions involved in this paper, a channel length of 1.5 m, a channel width of 4 mm, Re_{in} of 1483, and an a value of 0.33 are recommended.
(3) The reinforcement factor η/η_0 introduced in this paper can indicate the economy of improvement measures to the prototype. In the condition suggested by this paper, η/η_0 closes to 1.2.

The simplified method will facilitate the 3-D numerical calculation of DIEC. In the future, further improvements on the limitations of the current model will be carried out.

Author Contributions: W.Z.: Writing—review and editing. L.W.: Methodology. Y.J.: Writing—original draft. All authors have read and agreed to the published version of the manuscript.

Funding: This research was funded by the Key Research and Development Program of Gansu Provincial Science and Technology Plan, grant number 26YFFA045, covering the research period from March 2026 to February 2028.

Data Availability Statement: The data will be made available upon request.

Acknowledgments: During the preparation of this work, the author used ChatGPT 6.0 to improve language readability and fluency. After using this tool, the author reviewed and edited the content as needed and took full responsibility for the content of the publication.

Conflicts of Interest: The authors declare no conflict of interest.

Nomenclature

a	the air ratio of the secondary air in the wet channel to the primary air in the dry channel
A	the heat exchange area, m^2
c_p	the specific heat at constant pressure, J/(kg·K)
C_v	the vapor concentration, mol/m^3
d	the equivalent diameter, m
D	the diffusion coefficient of water vapor in air, m^2/s
f	the resistance factor
f_0	the resistance factor of the referenced DIEC [20,21]
F	the volume force vector, N/m^3
g_v	Mass transfer flux of water vapor, $kg/(m^2 \cdot s)$
h	the channel height, m
I	the identity matrix (unincorporated)
j	the heat transfer factor

j_0	the heat transfer factor of the referenced DIEC [20,21]
K	Convective mass transfer coefficient, m/s
l	the channel length, m
$\dot{m}$	the mass flow of air, kg/s
M_v	the molar mass of water vapor, kg/mol
$\boldsymbol{n}$	the normal direction of q
Nu	Nusselt number
p	the pressure of air, Pa
Pr	Prandtl number
q	the cooling capacity per unit area obtained by the product air, W/m^2
Re	Reynolds number
t	the time, s
T	the temperatures, K
T_f	the water film temperature, K
$\mathbf{U}$	the velocity vector, m/s
w	the channel width, m
ΔP	the resistance loss, Pa
δ	the plate thickness, mm
η	the efficiency
η_0	the efficiency of the referenced DIEC [20,21]
λ	the thermal conductivity of the plate, W/(m·K)
μ	the moist air dynamic viscosity, Pa·s
ρ	the density of air, kg/m^3
τ	the viscous stress tensor, Pa
φ_w	the relative humidity of air, %RH
subscript	
0	the referenced model and method
dc	the dry channel
dp	the dew point of water vapor
f	the water film
in	the inlet
out	the outlet
s,d	the wall surface at the dry channel
s,w	the wall surface at the wet channel
sat·T	the saturation state at T temperature
v	the water vapor
w	the plate wall
wc	the wet channel

References

1. Pérez-Lombard, L.; Ortiz, J.; Pout, C. A review on buildings energy consumption information. *Energy Build.* **2008**, *40*, 394–398. [CrossRef]
2. Lee, J.; Choi, B.; Lee, D.Y. Comparison of configurations for a compact regenerative evaporative cooler. *Int. J. Heat Mass Transf.* **2013**, *65*, 192–198. [CrossRef]
3. Uçkan, İ.; Yılmaz, T.; Hürdoğan, E.; Büyükalaca, O. Experimental investigation of a novel configuration of desiccant based evaporative air conditioning system. *Energy Convers. Manag.* **2013**, *65*, 606–615. [CrossRef]
4. Zhu, G.; Wen, T.; Wang, Q.; Xu, X. A review of dew-point evaporative cooling: Recent advances and future development. *Appl. Energy* **2022**, *312*, 118785. [CrossRef]
5. Riangvilaikul, B.; Kumar, S. An experimental study of a novel dew point evaporative cooling system. *Energy Build.* **2010**, *42*, 637–644. [CrossRef]
6. Bruno, F. On-site experimental testing of a novel dew point evaporative cooler. *Energy Build.* **2011**, *43*, 3475–3483. [CrossRef]
7. Lee, J.; Lee, D.Y. Experimental study of a counter flow regenerative evaporative cooler with finned channels. *Int. J. Heat Mass Transf.* **2013**, *65*, 173–179. [CrossRef]

8. Duan, Z.; Zhan, C.; Zhao, X.; Dong, X. Experimental study of a counter-flow regenerative evaporative cooler. *Build. Environ.* **2016**, *104*, 47–58. [CrossRef]
9. Duan, Z.; Zhao, X.; Zhan, C.; Dong, X.; Chen, H. Energy saving potential of a counter-flow regenerative evaporative cooler for various climates of China: Experiment-based evaluation. *Energy Build.* **2017**, *148*, 199–210. [CrossRef]
10. Chen, Y.; Yang, H.X.; Luo, Y.M. Indirect evaporative cooler considering condensation from primary air: Model development and parameter analysis. *Build. Environ.* **2016**, *95*, 330–345. [CrossRef]
11. Hasan, A. Going below the wet-bulb temperature by indirect evaporative cooling: Analysis using a modified ε-NTU method. *Appl. Energy* **2012**, *89*, 237–245.
12. Jradi, M.; Riffat, S. Experimental and numerical investigation of a dew-point cooling system for thermal comfort in buildings. *Appl. Energy* **2014**, *132*, 524–535. [CrossRef]
13. Pandelidis, D.; Anisimov, S. Numerical analysis of the heat and mass transfer processes in selected M-Cycle heat exchangers for the dew point evaporative cooling. *Energy Convers. Manag.* **2015**, *90*, 62–83. [CrossRef]
14. Wan, Y.; Lin, J.; Chua, K.J.; Ren, C. A new method for prediction and analysis of heat and mass transfer in the counter-flow dew point evaporative cooler under diverse climatic, operating and geometric conditions. *Int. J. Heat Mass Transf.* **2018**, *127*, 1147–1160. [CrossRef]
15. Pakari, A.; Ghani, S. Comparison of 1D and 3D heat and mass transfer models of a counter flow dew point evaporative cooling system: Numerical and experimental study. *Int. J. Refrig.* **2019**, *99*, 114–125. [CrossRef]
16. Liu, Y.; Akhlaghi, Y.G.; Zhao, X.; Li, J. Experimental and numerical investigation of a high-efficiency dew-point evaporative cooler. *Energy Build.* **2019**, *197*, 120–130. [CrossRef]
17. Lin, J.; Wang, R.; Li, C.; Wang, S.; Long, J.; Chua, K.J. Towards a thermodynamically favorable dew point evaporative cooler via optimization. *Energy Convers. Manag.* **2020**, *203*, 112224. [CrossRef]
18. Baakeem, S.S.; Orfi, J.; Mohamad, A.A. Investigations of geometrical and operational aspects of a dew-point air-cooling system (M-cycle). *J. Build. Eng.* **2021**, *36*, 102117. [CrossRef]
19. Zhu, G.; Chen, W.; Zhang, D.; Wen, T. Performance evaluation of counter flow dew-point evaporative cooler with a three-dimensional numerical model. *Appl. Therm. Eng.* **2023**, *219*, 119483. [CrossRef]
20. He, Y.L.; Tang, S.Z.; Tao, W.Q.; Li, M.J.; Wang, F.L. A general and rapid method for performance evaluation of enhanced heat transfer techniques. *Int. J. Heat Mass Transf.* **2019**, *145*, 118780. [CrossRef]
21. Rosaguti, N.R.; Fletcher, D.F.; Haynes, B.S. Low-Reynolds number heat transfer enhancement in sinusoidal channels. *Chem. Eng. Sci.* **2007**, *62*, 694–702. [CrossRef]

Disclaimer/Publisher's Note: The statements, opinions and data contained in all publications are solely those of the individual author(s) and contributor(s) and not of MDPI and/or the editor(s). MDPI and/or the editor(s) disclaim responsibility for any injury to people or property resulting from any ideas, methods, instructions or products referred to in the content.